CHINESE OPTICS LETTERS

Vol. 21, No. 7 | July 2023

Constructing ultra-long focal fields via tightly focused Bessel beams

Zhaojin Guo (郭兆金), Mingshuai Huang (黄铭帅), Sheng Liu (刘 圣)*, Peng Li (李 鹏)**, Bingyan Wei (魏冰妍), and Jianlin Zhao (赵建林)

Key Laboratory of Light Field Manipulation and Information Acquisition, Ministry of Industry and Information Technology, Shaanxi Key Laboratory of Optical Information Technology, School of Physical Science and Technology, Northwestern Polytechnical University, Xi'an 710129, China

*Corresponding author: shengliu@nwpu.edu.cn

**Corresponding author: pengli@nwpu.edu.cn

Received February 13, 2023 | Accepted April 13, 2023 | Posted Online July 10, 2023

We numerically demonstrate that the tight focusing of Bessel beams can generate focal fields with an ultra-long depth of focus (DOF). The ultra-long focal field can be controlled by appropriately regulating the order of the Bessel function and the polarization. An optical needle and an optical dark channel with nearly 100λ DOF are generated. The optical needle has a DOF of ~104.9λ and a super-diffraction-limited focal spot with the size of 0.19λ^2. The dark channel has a full-width at half-maximum of ~0.346λ and a DOF of ~103.8λ. Furthermore, the oscillating focal field with an ultra-long DOF can be also generated by merely changing the order of the input Bessel beam. Our results are expected to contribute to potential applications in optical tweezers, atom guidance and capture, and laser processing.

Keywords: Bessel beam; vector beam; tight focusing; depth of focus.

DOI: 10.3788/COL202321.072601

1. Introduction

Bessel beams are spatially structured beams with diffraction-free properties[1,2]. In recent years, Bessel beams have been extensively studied due to their non-diffracting and self-healing properties and have been used for exploring novel features and applications, such as generating light bullets with non-spreading features in a space–time domain[3], enhancing the imaging quality[4], conveying particles backward or forward[5], realizing polarization rotation along propagation direction[6,7], and producing frozen waves with arbitrarily tunable axial envelopes[8–10]. Furthermore, their accelerating property also has become one of the important extensions of Bessel beams. Unlike the conventional Bessel beams that propagate in a straight line, many types of quasi-Bessel beams that propagate along predefined trajectories, including the spiral line[11], the snake-shaped line[12], and even an arbitrary curve[13,14], have been proposed. A decade ago, Bessel beam propagating along a circular trajectory had been proposed in the nonparaxial region [15,16]. Based on this nonparaxial accelerating beam, we have recently proposed a new type of autofocusing beam, i.e., a tightly autofocusing beam[17]. The longitudinal field of the tightly autofocusing beam can be greatly enhanced by employing cylindrical polarization.

Cylindrically polarized beams, generally called cylindrical vector beams, have received considerable attention in recent decades because of their unique focusing characteristics[18–23]. Radially and azimuthally polarized beams are two typical cylindrical vector beams. After focusing, the former can generate a strong longitudinal electric field component using a high numerical aperture (NA) aplanatic lens, of which the spot size is smaller than the conventional optical diffraction limit. While the latter has a strong longitudinal magnetic field component. These focusing properties have a wide range of applications in many fields, such as quantum optics and information[24], laser micromachining[25], super-resolution microscopy[26], and second-harmonic generation[27]. On the other hand, the focusing field manipulation is a hot research topic of vector beams. In many research, the focal fields with special structures, including an optical needle[28], an optical cage[29], a flattop field[30], and an optical dark channel[31], are created by modulating the polarization, amplitude, and phase of the beam. The optical needle has a non-diffraction property and an ultra-long depth of focus (DOF). These properties have shown tremendous potential for various practical applications, such as optical lithography[32], optical data storage[33], and high-resolution optical imaging[34]. Moreover, different optical elements, such as the Pancharatnam–Berry phase element[35], the spatial light modulator[36], periodically poled crystals[37], and metalenses[38], are employed to experimentally generate the ultra-long focus field. To increase the length of the optical needle, several methods are proposed, including high NA objective lenses with a diffractive

optical element (DOE)[39,40], a spherical mirror[41], a Fresnel zone plate[42], artificial neural networks[43], and a phase mask[44]. In addition, different spatially structured beams have been used as the incident beam to generate optical needles[45,46]. Particularly, the circular Airy beam with autofocusing properties has been reported to generate a super long optical needle and a dark channel when focused with a high NA lens[47]. Revealing the tightly focusing properties of other structured beams is still an ongoing research topic.

In this work, we investigate the tight focusing of cylindrically polarized Bessel beams (CPBBs) using a high NA lens based on Richards–Wolf vector diffraction theory. By tuning the order of the Bessel function and the polarization of the beam, an optical needle, an optical dark channel, and an oscillating focal field are generated, all of which have ultra-long DOFs. The focusing properties, including the full-width at half-maximum (FWHM), the polarization, and the DOF, are discussed in detail. It reveals that as the order of the input Bessel beam increases, the optical needle and the FWHM decrease. These results are expected to contribute to potential applications in optical tweezers, atom guidance and capture, and laser processing.

2. Theoretical Principle

The schematic of the CPBB focused using a high NA aplanatic lens is shown in Fig. 1, where the left side represents the intensity distributions of the CPBBs with radial and azimuthal polarizations, and the green and blue markers depict the change process of the radial and azimuthal polarization, respectively. The electric fields near the focal plane can be derived from the Richards–Wolf vector diffraction theory[18]. The electric field components near the focus can be expressed as

$$\begin{bmatrix} E_r \\ E_\varphi \\ E_z \end{bmatrix} = A \int_0^{\theta_{\max}} l(\theta)\mathbf{p}(\theta)\sqrt{\cos\theta}\exp(ikz\cos\theta)\mathrm{d}\theta, \quad (1)$$

where the polarization vector $\mathbf{p}$ is

$$\mathbf{p} = \begin{bmatrix} \cos\varphi_0 \sin\theta\cos\theta J_1(kr\sin\theta) \\ \sin\varphi_0 \sin\theta J_1(kr\sin\theta) \\ i\cos\varphi_0 \sin^2\theta J_0(kr\sin\theta) \end{bmatrix}. \quad (2)$$

Here, (r, φ, z) are the cylindrical coordinates in the focal field, E_r, E_φ, and E_z denote the three components along the coordinates, A is a constant meeting of $A = kf$, f is the focal length of the lens, $k = 2\pi/\lambda$ is the wave number in the vacuum, φ_0 decides the polarization state of the incident beam, $\theta_{\max}$ is the maximum aperture angle determined by the lens and meets $\theta_{\max} = \sin^{-1}(\mathrm{NA})$, $l(\theta)$ is the amplitude distribution of the input beam, and $J_n(\cdot)$ denotes the n-order Bessel function of the first kind. We chose the incident CPBB, which is expressed as[17]

$$l(\theta) = J_\beta(kf\sin\theta)\exp(-\alpha f\sin\theta), \quad (3)$$

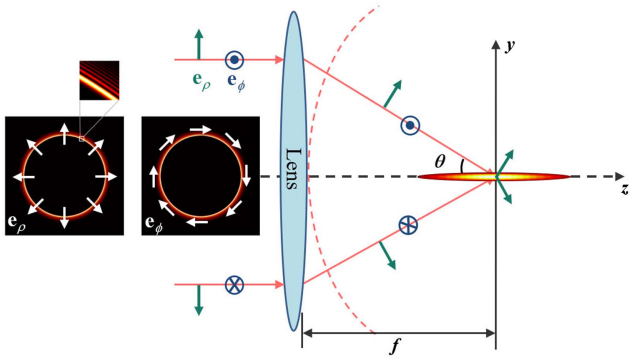

Fig. 1. Schematic of the tight focusing of the CPBB, where the insets denote the amplitude and the polarization profiles of the input beam, the green and blue markers denote the radial ($\mathbf{e}_\rho$) and azimuthal ($\mathbf{e}_\varphi$) polarizations, and θ denotes the angle between the focused ray and the z-axis.

where β is the order of the Bessel function, and α is a decay parameter, which guarantees the finite energy. Here, the order β can mainly regulate the radius of the main lobe of the input of the CPBB, which can be set as an arbitrary positive real number. Substituting Eq. (3) into Eq. (1), one can calculate the amplitude distributions of the three polarization components of the focal field. As shown in Eq. (1), some parameters of the focusing system affect the intensity distribution remarkably. In the following, we will analyze the influence of the order β and the incident polarization on the focusing characteristics of the CPBBs.

3. Results and Discussion

First, we investigate the tight focusing properties of the radially polarized ($\varphi_0 = 0$) CPBB through a high NA aplanatic lens. We set the parameters as follows: NA = 0.95, $\lambda = 633$ nm, $f = 240\,\mu$m, $\alpha = 10^5\mathrm{m}^{-1}$, $\beta = 1700$. Figures 2(a)–2(c) depict

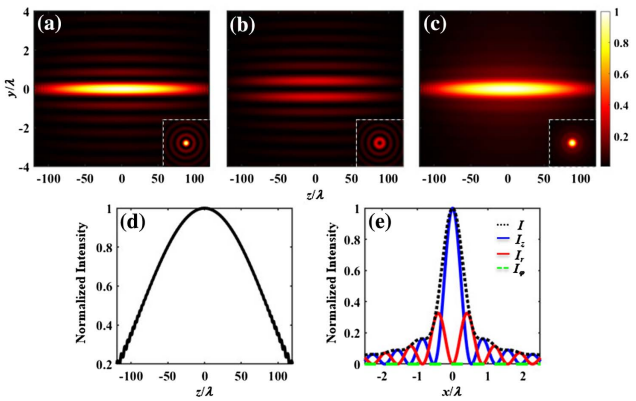

Fig. 2. Optical needle is generated by the tightly focused CPBB. (a)–(c) The intensity distributions of the longitudinally and radially polarized components and the total field in yz-plane, with the transverse focal spots within 5λ squared areas inserted. (d) The intensity profile of the optical needle along the z-axis. (e) The total field, radially, and longitudinally polarized components in the focal plane.

the intensity distributions (normalized by the total peak intensity) of the longitudinally (I_z) and radially (I_r) polarized components and the total field (I), respectively, where the insets show the corresponding transverse spot in the focal plane ($z = 0$). Figure 2(d) shows the total intensity profile along the z-axis, and Fig. 2(e) depicts the normalized transverse intensity distribution profiles of I, I_r, and I_z. The longitudinal and radial components are better able to maintain the shape during transmission over a rather long distance. The longitudinal component resembles a zero-order Bessel beam, while the intensity distribution of the radial component looks like the first-order one. The ratio of the peak intensity of the longitudinal component to that of the radial one is ~3.06. Since the radial component is weaker, the focal field forms a long optical needle of 170.26λ. In addition, the FWHM of the optical needle is 0.736λ, and the spot size is calculated as 0.425λ^2. The optical needle with an ultra-long DOF would have potential applications in many practical applications, such as nano-lithography, super resolution imaging, and data storage.

The optical needle can be affected by the order of the input Bessel beam. Figure 3(a) shows the FWHM and the peak intensity ratio between the longitudinal and radial components of the optical needle versus the order β. With the increase of β, the FWHM decreases, while the ratio of $I_{z\max}/I_{r\max}$ increases. Namely, a larger β generates an optical needle with a higher aspect ratio. As can be seen from the numerical results, the transverse dimension of the beam can reach diffraction limit size.

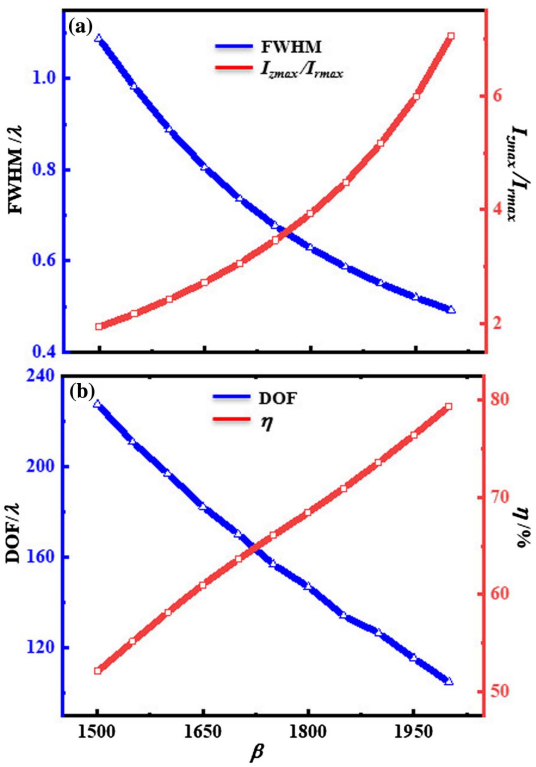

Fig. 3. The focusing properties of the optical needle in the focal plane versus β. (a) The FWHM and ratio of I_{zmax}/I_{rmax}. (b) The DOF and energy proportion (η).

Figure 3(b) shows the DOF versus β, as well as the energy proportion η of the longitudinal field. Here, η is defined as $\tau_z/(\tau_z + \tau_r)$, where $\tau_{r,z} = 2\pi\int|E_{r,z}|^2 r dr$. Clearly, this indicates that the CPBB with a larger β produces a stronger longitudinal field when it is tightly focused. More energy is assigned to the longitudinal field, which dominates the formation of the optical needle. This shows the possibility of creating ultra-long optical needles with small spot sizes in the longitudinal direction. When $\beta = 2000$, η is as high as 79.36%, the ratio of $I_{z\max}/I_{r\max}$ is 7.05, the spot size is 0.19λ^2, and the length of the optical needle reaches 104.88λ. As β continues to increase, the DOF would no longer increase, and the optical needle would turn into an oscillating field. Therefore, we need to choose the appropriate beam parameters to obtain the ultra-long optical needle.

Generally, the growth of the order β of the Bessel beam would increase the radius of the main lobe, and thus more side lobes would lie beyond the lens aperture. When β is large enough, the focal field of the CPBB would no longer be an optical needle but would become the longitudinal oscillating fields, as shown in Figs. 4(b)–4(e). The oscillating number can be precisely regulated by the number of ring lobes of the CPBB inside the lens aperture. As shown in the Fig. 4(a), when $\beta = 2158$, 2180, and 2206, the ring numbers of the CPBBs are 7, 5, and 3, respectively. We could see from Figs. 4(b)–4(e) that the peak number of the longitudinal oscillation is exactly equal to the ring number.

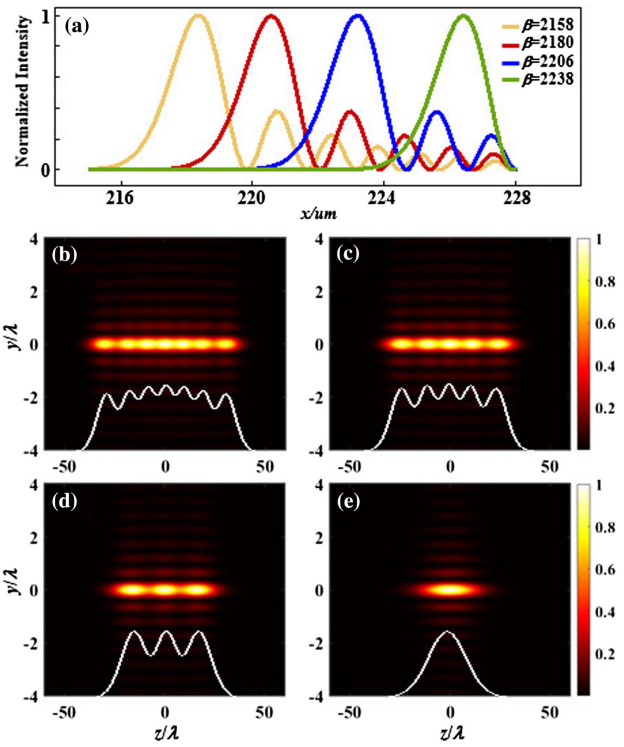

Fig. 4. Optical needle with longitudinal oscillating profiles. (a) The profiles of the input CPBBs with different β, where the abscissa has reached the upper limit. (b)–(e) The normalized intensity distribution and intensity profile of the total field in yz-plane when β = 2158, 2180, 2206, and 2238 with an NA = 0.95, respectively.

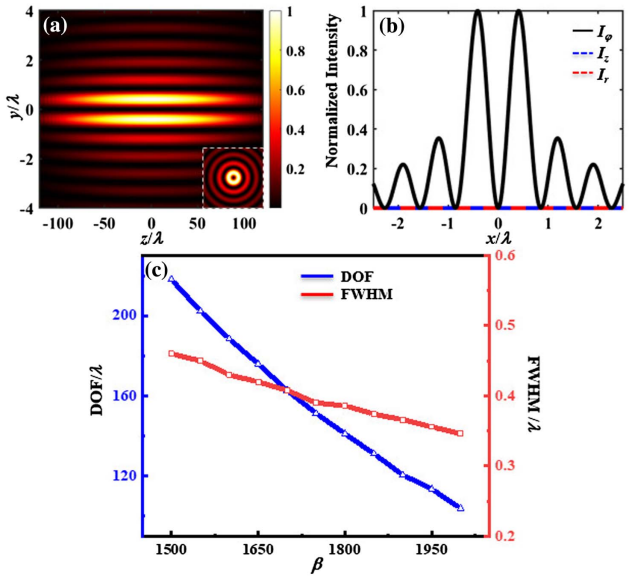

Fig. 5. Optical dark channel is generated by the tightly focused CPBB. (a) The intensity distribution of the total field in the *yz*-plane, with the transverse focal spots inserted. (b) The transverse intensity distribution of the azimuthally, radially, and longitudinally polarized components at the focal plane. (c) The DOF and the FWHM of the focal plane versus β.

The intensity of the oscillating field gradually decreases when it moves away from the focal plane. The oscillating phenomenon arises mainly from the interference between the optical needles generated by the focusing of the ring-shape lobes, where the adjacent ones are out of phase, since these ring-shaped lobes have different radii. They produce optical needles with different DOFs when focused by the objective lens. The interference of these optical needles forms the oscillation field, especially when $\beta = 2238$ and the ring number of the CPBB is only 1. The focal field produces an optical needle with a DOF of $\sim 21.97\lambda$ and a FWHM of $\sim 0.38\lambda$, which is longer than that generated from the radially polarized, narrow-width annular beam[48]. It is important to note that when more than enough ring lobes participate in the focusing, the oscillation is not necessarily noticeable but could be dimly seen, as shown in Fig. 2(d). The controllable oscillation peak in the focal field might help to orderly arrange the particles for the application of the optical tweezer when it is used to capture multiple particles.

Next, the focusing property of the azimuthally polarized beam is investigated, where the parameters are the same as that in Fig. 2, except $\varphi_0 = 90°$. Figure 5(a) depicts the normalized intensity distribution of the total field in the *yz* plane and the transverse focal spot (see the inset). The focal field resembles the first-order Bessel beam and behaves as an ultra-long dark channel, of which the DOF is about 162.75λ. Figure 5(b) shows the normalized transverse intensity distribution profiles of I_φ, I_r, and I_z at the focal plane. The focal field has only the azimuthally polarized component, where the FWHM of the dark core has a sub-diffraction size of 0.41λ. Compared with the dark channel generated by focusing a double-ring-shaped azimuthally polarized beam with a high NA lens axicon[49], of which the FWHM is 0.5λ and the DOF is 48λ, the dark channel of our method is narrower and longer. Figure 5(c) depicts the FWHM and the DOF of the dark channel versus β, revealing that the DOF and the FWHM gradually decrease as β increases. An ultra-long dark channel with a FWHM of $\sim 0.346\lambda$ and a DOF of $\sim 103.81\lambda$ at $\beta = 2000$ can be generated using our method. The ultra-long dark channel will be useful for atom guiding[50].

4. Conclusion

In conclusion, we have investigated the CPBBs that have been tightly focused using a high NA aplanatic lens. By modulating the polarization and the order of the Bessel function, we can construct the ultra-long focus field. Numerical results show that the optical needle and dark channel with nearly 100λ DOF could be generated. The optical needle can be tuned into the longitudinal oscillating focal field with appropriate parameters. By further changing the order, we can easily regulate the DOF and FWHM of the optical needle and the optical dark channel. We believe that this work will help to explore the properties of the tight focusing of vector beams.

Acknowledgement

This work was supported by the National Key Research and Development Program of China (No. 2022YFA1404800), National Natural Science Foundation of China (NSFC) (Nos. 12074312, 11634010, 12074313, and 12174309), Fundamental Research Funds for the Central Universities (No. 3102019JC008), and Innovation Foundation for Doctor Dissertation of Northwestern Polytechnical University (No. CX2021115).

References

1. J. Durnin, "Exact solutions for nondiffracting beams. I. The scalar theory," J. Opt. Soc. Am. A **4**, 651 (1987).
2. J. Durnin, J. J. Miceli, Jr., and J. H. Eberly, "Diffraction-free beams," Phys. Rev. Lett. **58**, 1499 (1987).
3. A. Chong, W. H. Renninger, D. N. Christodoulides, and F. W. Wise, "Airy–Bessel wave packets as versatile linear light bullets," Nat. Photonics **4**, 103 (2010).
4. F. O. Fahrbach and A. Rohrbach, "Propagation stability of self-reconstructing Bessel beams enables contrast-enhanced imaging in thick media," Nat. Commun. **3**, 632 (2012).
5. D. B. Ruffner and D. G. Grier, "Optical conveyors: a class of active tractor beams," Phys. Rev. Lett. **109**, 163903 (2012).
6. S. Liu, S. Qi, P. Li, B. Wei, P. Chen, W. Hu, Y. Zhang, X. Gan, P. Zhang, Y. Lu, Z. Chen, and J. Zhao, "Analogous optical activity in free space using a single Pancharatnam–Berry phase element," Laser Photonics Rev. **16**, 2100291 (2022).
7. P. Li, Y. Zhang, S. Liu, L. Han, H. Cheng, F. Yu, and J. Zhao, "Quasi-Bessel beams with longitudinally varying polarization state generated by employing spectrum engineering," Opt. Lett. **41**, 4811 (2016).
8. T. A. Vieira, M. R. R. Gesualdi, and M. Zamboni-Rached, "Frozen waves: experimental generation," Opt. Lett. **37**, 2034 (2012).

9. A. H. Dorrah, M. Zamboni-Rached, and M. Mojahedi, "Generating attenuation-resistant frozen waves in absorbing fluid," Opt. Lett. **41**, 3702 (2016).
10. R. A. B. Suarez, L. A. Ambrosio, A. A. R. Neves, M. Zamboni-Rached, and M. R. R. Gesualdi, "Experimental optical trapping with frozen waves," Opt. Lett. **45**, 2514 (2020).
11. V. Jarutis, A. Matijošius, P. Di Trapani, and A. Piskarskas, "Spiraling zero-order Bessel beam," Opt. Lett. **34**, 2129 (2009).
12. J. E. Morris, T. Čižmár, H. I. C. Dalgarno, R. F. Marchington, F. J. Gunn-Moore, and K. Dholakia, "Realization of curved Bessel beams: propagation around obstructions," J. Opt. **12**, 124002 (2010).
13. J. Zhao, P. Zhang, D. Deng, J. Liu, Y. Gao, I. D. Chremmos, N. K. Efremidis, D. N. Christodoulides, and Z. Chen, "Observation of self-accelerating Bessel-like optical beams along arbitrary trajectories," Opt. Lett. **38**, 498 (2013).
14. J. Zhao, P. Zhang, D. Deng, C. Lou, D. Song, J. Liu, and Z. Chen, "Self-accelerating and self-breathing Bessel-like beams along arbitrary trajectories," Chin. Opt. Lett. **11**, 110701 (2013).
15. P. Zhang, Y. Hu, D. Cannan, A. Salandrino, T. Li, R. Morandotti, X. Zhang, and Z. Chen, "Generation of linear and nonlinear nonparaxial accelerating beams," Opt. Lett. **37**, 2820 (2012).
16. I. Kaminer, R. Bekenstein, J. Nemirovsky, and M. Segev, "Nondiffracting accelerating wave packets of Maxwell's equations," Phys. Rev. Lett. **108**, 163901 (2012).
17. S. Liu, Z. Guo, P. Li, B. Wei, and J. Zhao, "Tightly autofocusing beams: an effective enhancement of longitudinally polarized fields," Opt. Lett. **45**, 575 (2020).
18. Q. Zhan, "Cylindrical vector beams: from mathematical concepts to applications," Adv. Opt. Photonics **1**, 1 (2009).
19. L. Han, S. Qi, S. Liu, H. Cheng, P. Li, and J. Zhao, "Tightly focused light field with controllable pure transverse polarization state at the focus," Opt. Lett. **45**, 6034 (2020).
20. W. Zhang, S. Liu, P. Li, X. Jiao, and J. Zhao, "Controlling the polarization singularities of the focused azimuthally polarized beams," Opt. Express **21**, 974 (2013).
21. M.-S. Wang, X.-Z. Gao, J.-H. Zhao, X.-F. Sun, Y. Pan, and Y. Xia, "Flexibly modulated Poincaré sphere vector optical field in input and focal planes," Opt. Express **29**, 21071 (2021).
22. C. Zhang, C. Min, Y. Zhang, Y. Fu, L. Li, Y. Wang, and X. Yuan, "Detection of cylindrical vector beams with chiral plasmonic lens," Chin. Opt. Lett. **20**, 023602 (2022).
23. Z.-X. Li, Y.-P. Ruan, P. Chen, J. Tang, W. Hu, K.-Y. Xia, and Y.-Q. Lu, "Liquid crystal devices for vector vortex beams manipulation and quantum information applications [Invited]," Chin. Opt. Lett. **19**, 112601 (2021).
24. V. Parigi, V. D'Ambrosio, C. Arnold, L. Marrucci, F. Sciarrino, and J. Laurat, "Storage and retrieval of vector beams of light in a multiple-degree-of-freedom quantum memory," Nat. Commun. **6**, 7706 (2015).
25. H. Cheng, P. Li, S. Liu, P. Chen, L. Han, Y. Zhang, W. Hu, and J. Zhao, "Vortex-controlled morphology conversion of microstructures on silicon induced by femtosecond vector vortex beams," Appl. Phys. Lett. **111**, 141901 (2017).
26. Z. J. Hua, J. Liu, and C. G. Liu, "High-resolution dark-field confocal microscopy based on radially polarized illumination," Opt. Express **30**, 11066 (2022).
27. A. Bouhelier, M. Beversluis, A. Hartschuh, and L. Novotny, "Near-field second-harmonic generation induced by local field enhancement," Phys. Rev. Lett. **90**, 013903 (2003).
28. H. Wang, L. Shi, B. Lukyanchuk, C. Sheppard, and C. T. Chong, "Creation of a needle of longitudinally polarized light in vacuum using binary optics," Nat. Photonics **2**, 501 (2008).
29. Z. Zhang, H. Fan, H.-F. Xu, J. Qu, and W. Huang, "Three-dimensional focus shaping of partially coherent circularly polarized vortex beams using a binary optic," J. Opt. **17**, 065611 (2015).
30. W. Chen and Q. Zhan, "Three-dimensional focus shaping with cylindrical vector beams," Opt. Commun. **265**, 411 (2006).
31. B. Tian and J. Pu, "Tight focusing of a double-ring-shaped, azimuthally polarized beam," Opt. Lett. **36**, 2014 (2011).
32. Z. Gan, Y. Cao, R. A. Evans, and M. Gu, "Three-dimensional deep sub-diffraction optical beam lithography with 9 nm feature size," Nat. Commun. **4**, 2061 (2013).
33. M. Gu, X. Li, and Y. Cao, "Optical storage arrays: a perspective for future big data storage," Light Sci. Appl. **3**, e177 (2014).
34. K. S. Youngworth and T. G. Brown, "Focusing of high numerical aperture cylindrical-vector beams," Opt. Express **7**, 77 (2000).
35. P. Gotovski, P. Šlevas, S. Orlov, O. Ulčinas, and A. Urbas, "Generation of an optical needle beam with a laser inscribed Pancharatnam–Berry phase element under imperfect conditions," Opt. Express **29**, 33331 (2021).
36. J. Chen and Q. Xu, "Superlong uniform light tunnel created by focusing radially polarized vortex beam," J. Appl. Phys. **124**, 043103 (2018).
37. Y. Zhu, H. Wang, Y. Zhang, D. Liu, W. Zhong, Z. Gao, G. Cui, Y. Lu, Y. Zhang, and M. Xiao, "Generation of an ultra-long sub-diffracted second-harmonic optical needle from a periodically poled $LiNbO_3$ crystal," Appl. Phys. Lett. **116**, 081106 (2020).
38. Y. Zheng, M. Xu, M. Pu, F. Zhang, D. Sang, Y. Guo, X. Li, X. Ma, and X. Luo, "Designing high-efficiency extended depth-of-focus metalens via topology-shape optimization," Nanophotonics **11**, 2967 (2022).
39. K. Huang, P. Shi, X. Kang, X. Zhang, and Y. Li, "Design of DOE for generating a needle of a strong longitudinally polarized field," Opt. Lett. **35**, 965 (2010).
40. Z. Man, C. Min, L. Du, Y. Zhang, S. Zhu, and X. Yuan, "Sub-wavelength sized transversely polarized optical needle with exceptionally suppressed side-lobes," Opt. Express **24**, 874 (2016).
41. D. Panneton, G. St-Onge, M. Piché, and S. Thibault, "Needles of light produced with a spherical mirror," Opt. Lett. **40**, 419 (2015).
42. T. Liu, J. B. Tan, J. Liu, and H. Wang, "Modulation of a super-Gaussian optical needle with high-NA Fresnel zone plate," Opt. Lett. **38**, 2742 (2013).
43. W. Xin, Q. M. Zhang, and M. Gu, "Inverse design of optical needles with central zero-intensity points by artificial neural networks," Opt. Express **28**, 38718 (2020).
44. X.-Z. Gao, P.-C. Zhao, J.-H. Zhao, X.-F. Sun, J.-J. Liu, F. Yang, and Y. Pan, "Sinusoidal-amplitude binary phase mask and its application in achieving an ultra-long optical needle," Opt. Express **30**, 26275 (2022).
45. J. Lin, K. Yin, Y. Li, and J. Tan, "Achievement of longitudinally polarized focusing with long focal depth by amplitude modulation," Opt. Lett. **36**, 1185 (2011).
46. Z. Nie, G. Shi, X. Zhang, Y. Wang, and Y. Song, "Generation of super-resolution longitudinally polarized beam with ultra-long depth of focus using radially polarized hollow Gaussian beam," Opt. Commun. **331**, 87 (2014).
47. F. Wang, C. Zhao, Y. Dong, Y. Dong, and Y. Cai, "Generation and tight-focusing properties of cylindrical vector circular Airy beams," Appl. Phys. B **117**, 905 (2014).
48. K. Kitamura, K. Sakai, and S. Noda, "Sub-wavelength focal spot with long depth of focus generated by radially polarized, narrow-width annular beam," Opt. Express **18**, 4518 (2010).
49. K. Lalithambigai, P. Suresh, V. Ravi, K. Prabakaran, Z. Jaroszewicz, K. B. Rajesh, P. M. Anbarasan, and T. V. S. Pillai, "Generation of sub wavelength super-long dark channel using high NA lens axicon," Opt. Lett. **37**, 999 (2012).
50. Y. I. Shin, K. Kim, J. A. Kim, H. R. Noh, W. Jhe, K. Oh, and U. C. Paek, "Diffraction-limited dark laser spot produced by a hollow optical fiber," Opt. Lett. **26**, 119 (2001).